

## 2 Methods and Characterisation

### 2.1 Optical CT Materials and Methods

#### 2.1.1 Hardware

Our optical CT system is area-detector based, allowing for fast 3-D scanning. A high quality scientific Complementary Metal-Oxide Semiconductor (CMOS) camera (Zyla sCMOS, Andor Technology PLC, Belfast, UK) has excellent sensitivity, read-out noise and fast read-out speed.

We have two illumination sources. A flat-panel red Light Emitting Diode (LED) (PHLOX-LEDR-BL-100x100-S-Q-1R-24V, Phlox, Aix-en-Provence, France), with a wavelength of 633nm provides uniform lighting appropriate for imaging PRESAGE<sup>TM</sup>, a radiochromic plastic which has a strong absorption peak at 632nm. For tissue imaging the wavelength most appropriate for each sample is provided through the use of a new broadband white light source (SugarCUBE LED Illuminator, Nathaniel Group Inc., VT, USA) and tunable filter (VariSpec, PerkinElmer, Inc., MA, USA).

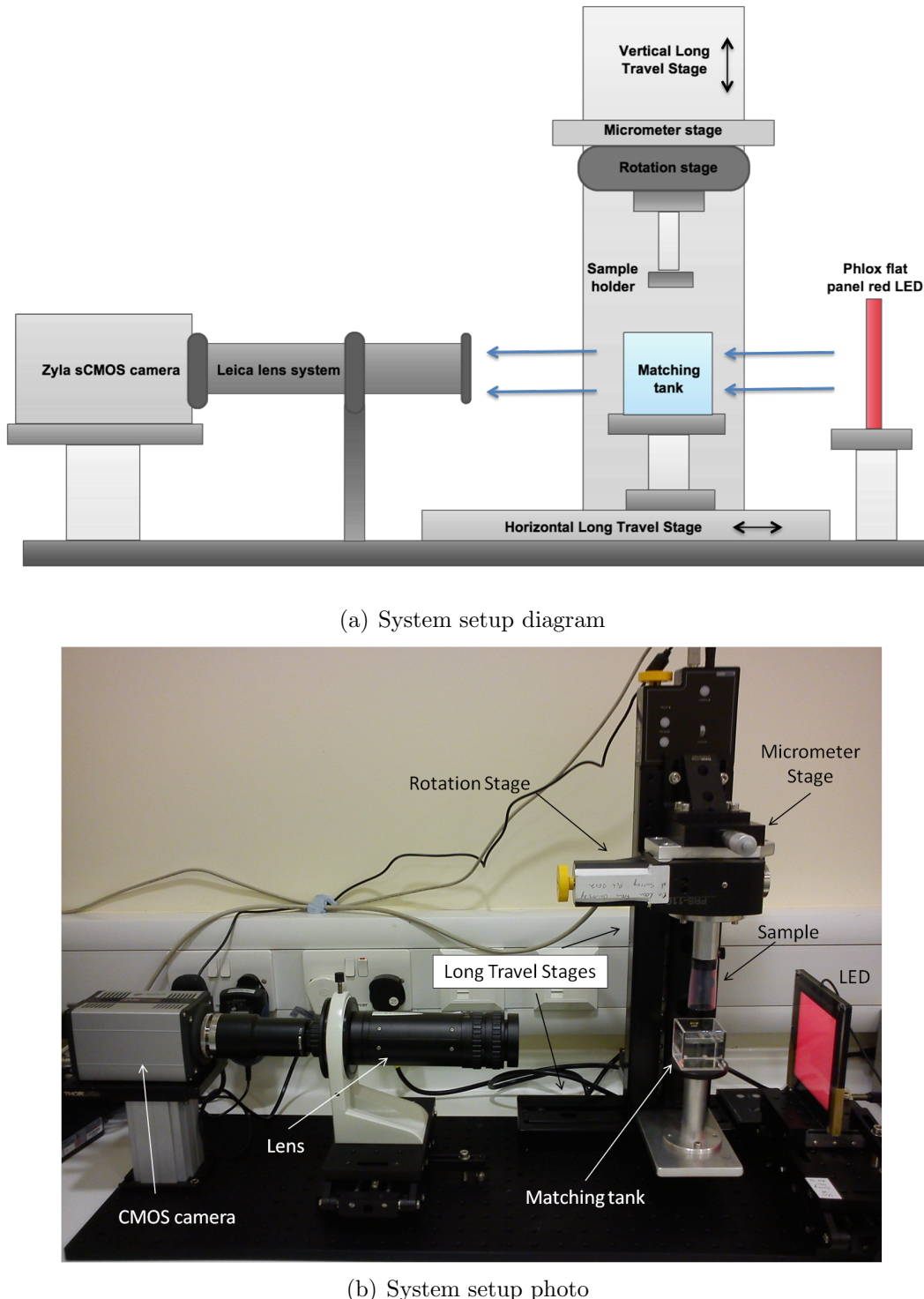


**Figure 2.1.** Diagram and picture of current set-up of optical CT system at the ICR with principal parts of apparatus labelled.

Samples are suspended from a rotary stage (PRS-110 ZSS43, PI miCos GmbH, Eschbach, Germany) in a glass matching tank (Part 704-002-40-10, Hellma GmbH, Müllheim, Germany). The COR can be adjusted through a micrometer stage

which moves the rotation stage. A COR-checker LabView program checks for accurate alignment of the COR with the centre of the FOV. Off-centre COR leads to artefacts which can be corrected as part of the reconstruction.

The matching tank is filled with ‘matching liquid’ with an RI close to that of the sample, avoiding refraction at the curved surface of the sample. For PRESAGE samples this matching fluid was a solution of (97% ethyl hexyl salicylate and 3% 4-methoxycinnamic acid 2-ethylhexyl ester) giving the same refractive index as the PRESAGE®. The clearing solution used for each tissue sample was used for matching fluid.

For initial measurements the rotation stage was supported on a large optical post. In an updated system this post was replaced with an Integrated Long Travel Stage (LTS-300/M, Thorlabs Ltd., Ely, UK ) which allows accurate and reproducible vertical positioning of samples. In collaboration with the ICR workshop, a novel mounting system has been developed to give reproducible positioning of samples allowing pre and post-irradiation scans of dosimetry gel. Two custom sample mounts are used for dosimetry and tissue samples respectively. The dosimetry mount fits caps that are fixed to PRESAGE samples, meaning the samples are in the same orientation for every scan. The tissue mount has two additional stages, giving the flexibility to position irregular samples on the COR independently of moving the COR.

An additional Long Travel Stage (LTS-150/M, Thorlabs LTD., Ely, UK ) allows accurate positioning of the sample and tank along the optical axis.

Light is collected by an imaging lens system made up of components of the modular ‘Z16 APO’ zoom system (Leica Microsystems GmbH, Wetzlar, Germany, see [Doran et al., 2010a] for details). The use of the zoom lens allows manual adjustment of the focus and magnification. However, in general the manual focus is left constant and we use the LTS stage to move the sample and tank along the optical axis for focusing - more repeatable. Add focusing protocol.

### 2.1.2 Software

#### Acquisition

Image acquisition and rotation are controlled synchronously by PC using an in-house program written in LabView (National Instruments Corporation Ltd., Berkshire, UK). The high capacity of the PC and camera allows for fast read-out

of images giving much reduced scan times to others previously reported. For standard scans images are acquired during continuous rotation of the sample.

If projections are acquired with no binning then a Step-and-shoot method with averaging of several projections is used to improve the SNR. This method takes much longer.

Include algorithms? Maybe in appendix?

## **Reconstruction**

Reconstruction is carried out via Filtered Back-projection (FBP) incorporating a ‘correction scan’ using in-house software written by SJD in IDL (Excelis Visual Information Solutions, Boulder, CO) (see [Doran et al., 2013b]).

‘Dark’ field (DF) and ‘light’ field (LF) images correct for structural noise in the camera and non-uniformities in the light path respectively. In general 30 DF (with cap on camera) and LF (no sample present) images were averaged for each scan and images are corrected during reconstruction according to equation (4) of Krstajić [Krstajić and Doran, 2007].

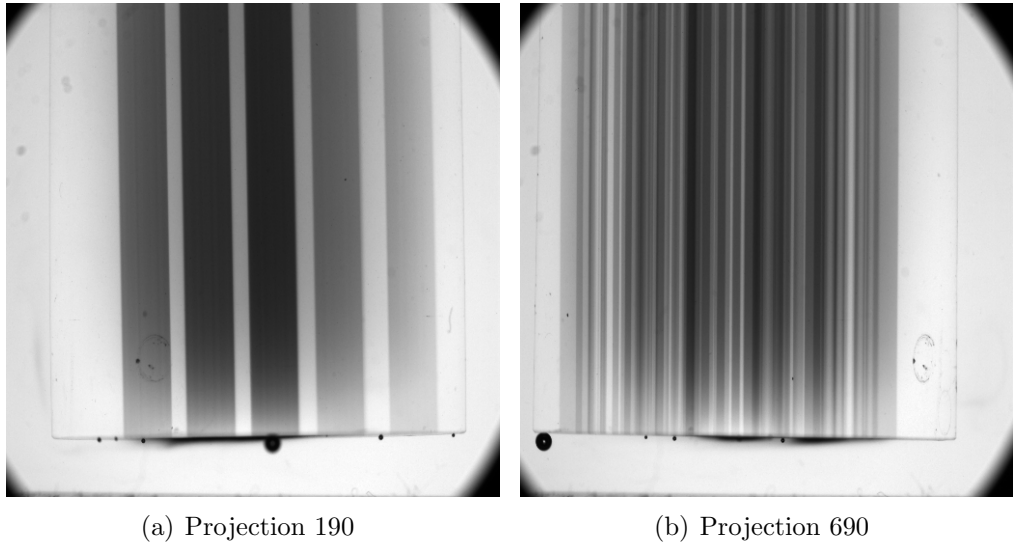
The software also allows for adjustment to correct for off-axis centre of rotation (COR). In the updated system the rotation stage is mounted on a micrometer stage allowing more precise alignment of the CoR. If the CoR is not aligned with the central pixel column then the sample will appear to drift across the screen and projection data will not be consistent for all angles. [Guo et al., 2006]

A ring artefact correction has been added to the reconstruction, based on [IN-SERT reference]. The number of pixels can be chosen depending on the matrix size of the projections.

### **2.1.3 Dosimetry protocol**

Optical CT imaging of PRESAGE samples was carried out in two modes. For qualitative visualisation of irradiation patterns fast scans were used, while samples for PVDR assessment were scanned with high-resolution scans. All scans had an aperture setting of A=1 so that the DOF encompassed the entire sample.

Scan	Projections	Pixels	Voxel size ( $\mu\text{m}$ )	Acquisition time
Fast	1000	$512 \times 512$	20.8	2.5 minutes
High-resolution	3200	$2048 \times 2048$	5.2	1 hour

**Table 2.1.** Different scanning parameters for MRT

**Figure 2.2.** Projections taken  $180^\circ$  apart through a PRESAGE<sup>TM</sup> sample irradiated at the ESRF with a defined test pattern of known line widths. Some air bubbles can be seen as dark circles at the base of the sample. Faint marks in the upper left parts of the images are caused by dust in the optics which will be corrected by a Light Field scan. In 2.2(b) a mark on the side of the sample itself can be seen near the bottom right. A small refractive index mismatch between the sample and liquid is seen by the faint outline of the sample walls. This will result in a circular artefact in reconstructed slices.

Projections, such as those seen in Figure 2.2 were reconstructed to give slices through the sample. A view through the sample made up of 20 averaged slices is seen in Figure 2.3. It was possible to average slices and thereby improve the SNR of the image because the sample was axially uniform. A clear dose pattern can be seen in the sample, similar to those previously reported by Doran *et al.* [Doran et al., 2013b]. Some blurring and ring artefacts can be seen but the overall image quality is good with high SNR. The RI mismatch artefact is not significant but could be improved. Lineprofiles for each row numbered on the slice are shown in Figure 2.4 showing how the system response falls off with increasing line-pairs per mm (lppm). A rolling baseline as previously reported by Doran is seen for line 3 whereby the signal falls off towards the edges of the sample.

The highest lppm pattern resolved was 20 lppm, seen on the far left of line 4. Three patterns on line 4 were not resolved representing 30, 40 and 50 lppm. This means the smallest resolvable object was between  $66\text{-}100\mu\text{m}$  and not  $40\mu\text{m}$  as predicted by the MTF data. This discrepancy is probably due a combination of blurring due to reconstruction, imperfect focusing and the fact that projections of the patterns are not always acquired with the pattern in the centre of the focal plane. The results from this phantom verified the optical CT system was working for dosimetry, allowing us to move onto adapting the system for imaging tissue.

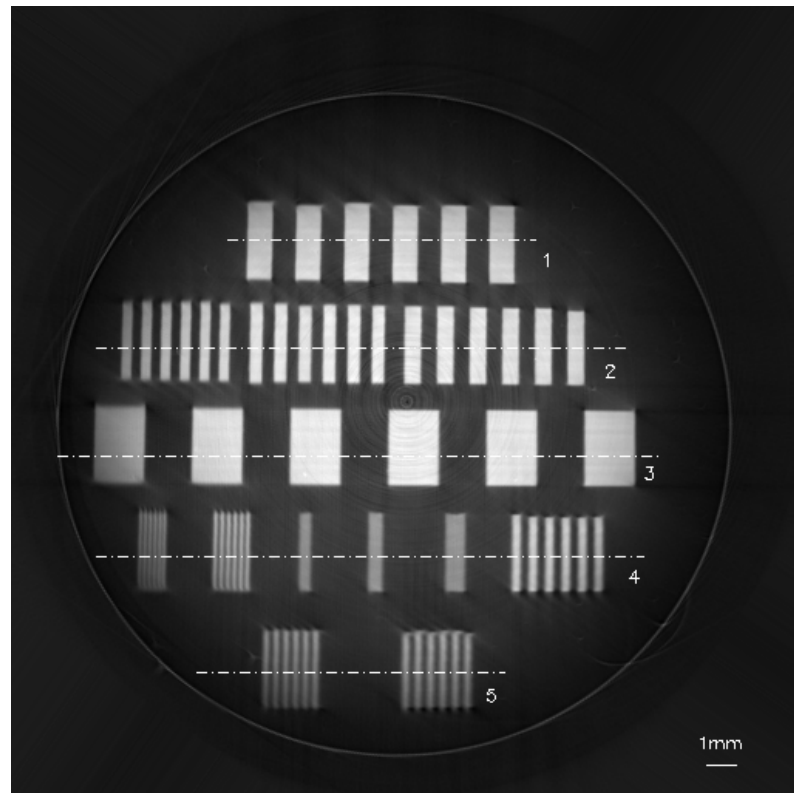


**Figure 2.3.** Reconstructed slice of the PRESAGE<sup>TM</sup> sample seen in Fig. 2.2. The image is a result of 20 averaged slices to improve the SNR. Annotations refer to line profiles plotted in Fig. 2.4.

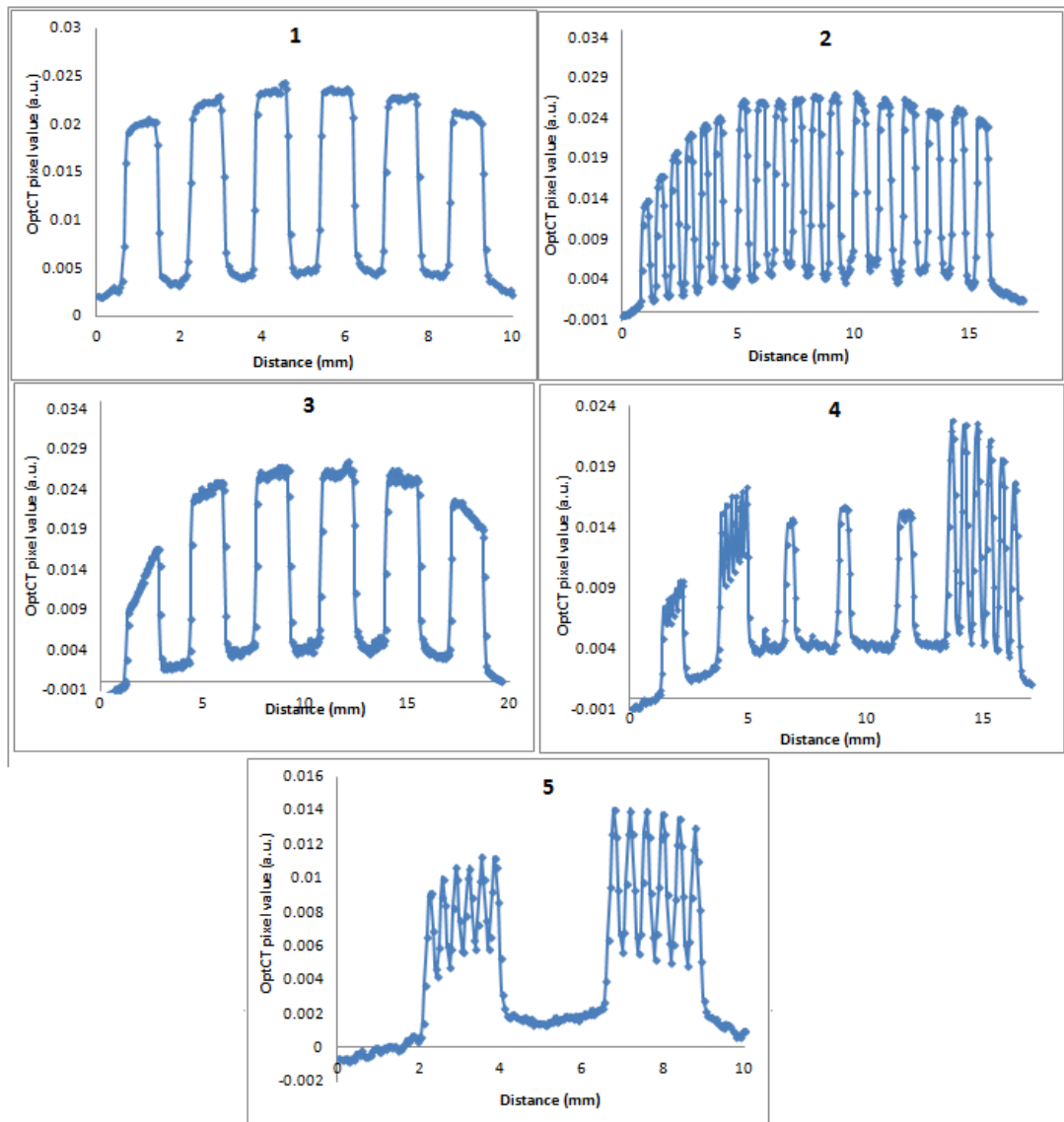


**Figure 2.4.** Lineprofiles for PRESAGE<sup>TM</sup> sample shown in Figure 2.3. The highest resolution pattern resolved was 20 lppm (far left of pattern 4) but the 30, 40 and 50 lpppm patterns on line 4 are unresolved. No modulation is seen for these patterns indicating that objects smaller than 100 $\mu$ m cannot be imaged.

#### 2.1.4 Tissue imaging protocol

Before imaging, tissue samples must undergo a series of preparation steps:

- Fix in 70% ethanol in phosphate-buffered saline (PBS) overnight
- Embed in 0.75% agarose for stability
- 3 – 4 washes of 100% ethanol

- Washes of 30% and 70% 1:2 benzyl benzoate:benzyl alcohol (BABB) in ethanol
- 1 – 2 washes of 100% 1:2 BABB (refractive index 1.559)
- Superglue agarose to sample holder prior to imaging with 1:2 BABB matching fluid.

Due to the small size and irregular shapes of tissue samples, a new positioning system was necessary to allow flexible positioning of samples on the centre of rotation. This is coupled with a LabView program for alignment makes sample positioning much easier, previously difficult and time consuming.

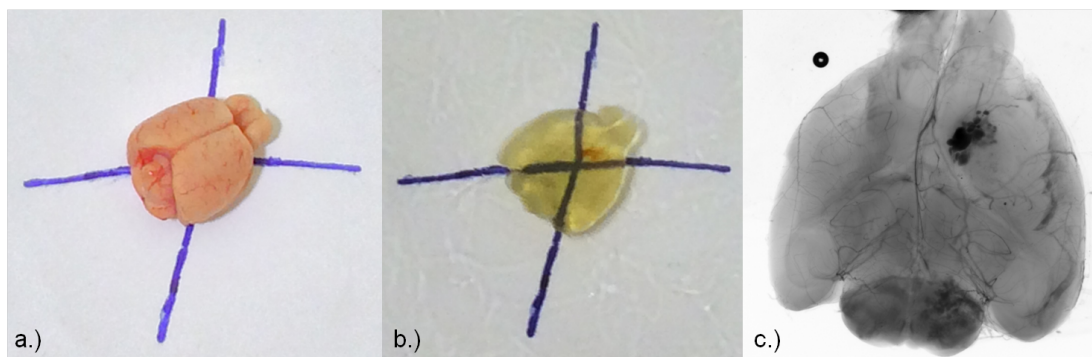


**Figure 2.5.** a.) Example of an uncleared mouse brain, b.) a cleared mouse brain in 1:2 BABB solution, c.) a projection image of the cleared brain mounted in the optical CT system.

Examples images of different healthy rodent organs are shown in Figure 2.6. Clearing with BABB has worked well and all contrast is endogenous. Clearing reduces light attenuation due to scattering, so any contrast is due to natural differences in light absorption properties between different tissue types. Highly attenuating areas, such as haemoglobin in the heart, or lipid-dense areas of the brain, are bright in these optical CT absorption scans.

Images of tissues containing tumours are shown in Figure 2.7, ranging from a large neuroblastoma tumour, of the order of 10mm, to a tumour cell spheroid around  $100\mu\text{m}$  diameter, at the extreme resolution limit of the system. It was noted that large and highly attenuating tissues (such as neuroblastoma tumours) required longer clearing time.

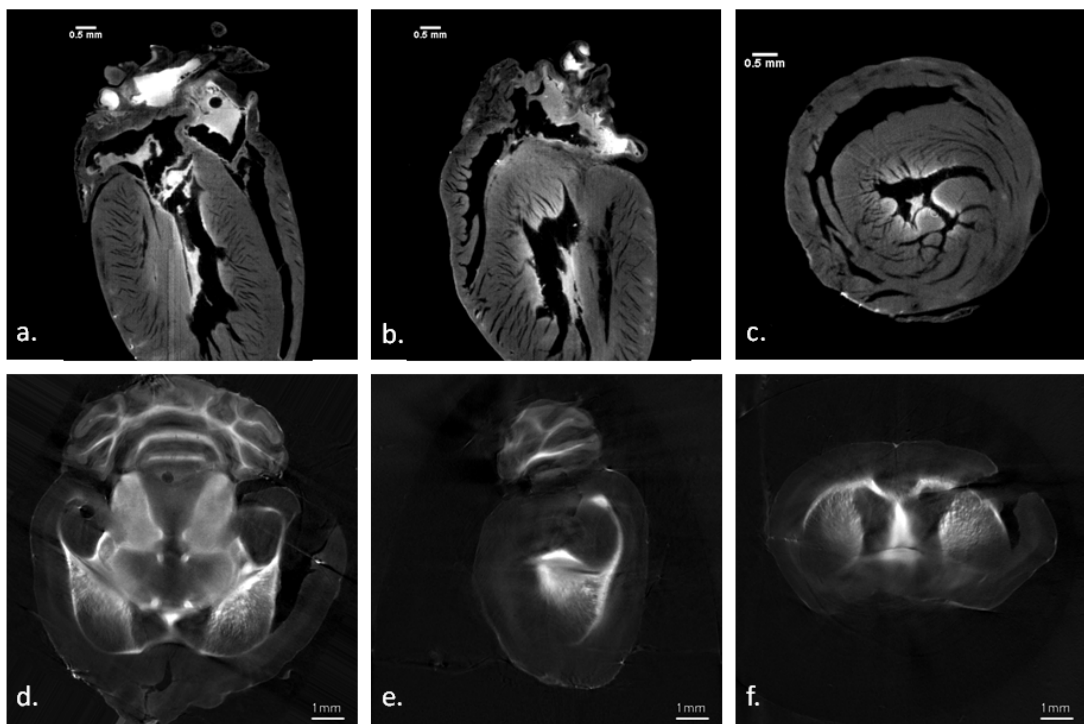


**Figure 2.6.** a-c.) Orthogonal slices of a reconstructed image volume of a mouse heart with endogenous contrast, most likely due to the presence of haemoglobin. d-f.) Orthogonal slices of a reconstructed image volume of a mouse brain where bright areas are likely due to attenuation due to lipid content of the brain. These images demonstrate high-resolution, highly detailed data reconstructed from absorption optical CT scans, without addition of external contrast.

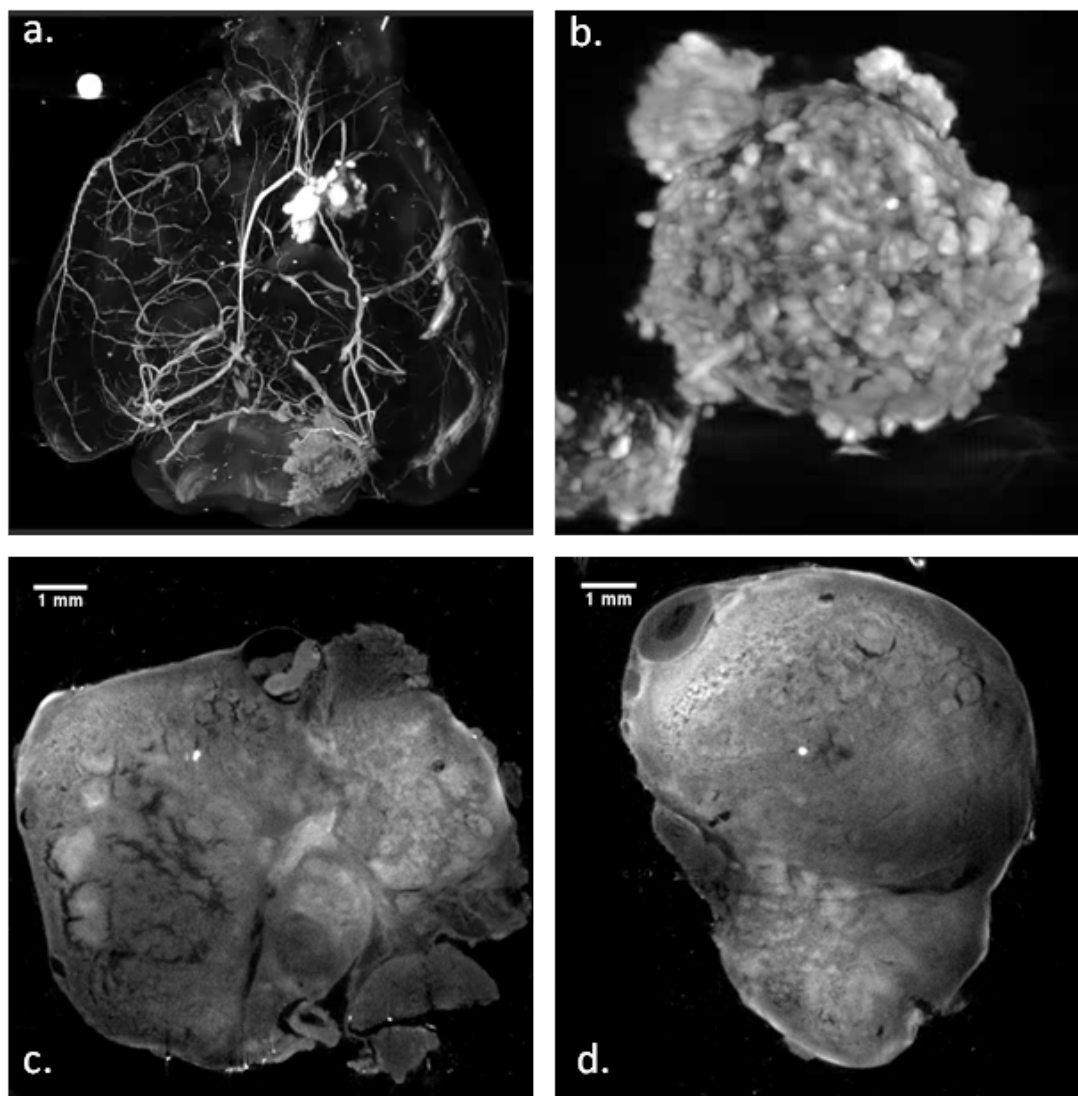


**Figure 2.7.** a.) Maximum intensity projection (MIP) of a mouse brain with an orthotopic glioblastoma tumour. A highly attenuating artefact due to an air bubble is seen in the top left corner. The mouse was injected with Evans Blue, an absorbing permeability marker which has stained the vasculature. The tumour was rich in haemoglobin and also appears very attenuating. This shows the potential for optical CT imaging of vasculature. b.) MIP image of a tumour cell spheroid stained with haematoxylin. c-d.) Orthogonal slices through a neuroblastoma tumour showing the detail possible using an anatomical scan. Additional functional information can be added with the use of fluorescent markers.

## 2.2 Optical CT system characterisation

### 2.2.1 Linear response

In order to establish the relationship between optical CT reconstructed pixel value and optical absorbance, gel finger phantoms were made in a similar fashion to [Oldham et al., 2003].

10% porcine gelatin (Sigma, REF) was made in water. Add exact method? Maybe in appendix. Heat to 60?deg, vacuum, stir while cooling to 25?.

A specialised finger phantom mould was made by the ICR workshop. A 3-D printed holder contained slots to hold metal rods on one side and can be attached directly to the rotation stage on the other. A cylinder of Teflon FEP heat-shrink plastic (Holscot Fluoroplastics Limited, Grantham, UK) was used to provide support for the gelatin. Teflon FEP has an RI of 1.341 making it a very close match for water and gelatin. [Krstajić and Doran, 2006] Cylindrical pieces of Teflon sleeving were cut a length of 4cm, the height of the matching tank and one end was heat shrunk onto the plastic mould providing a secure support for the cooling gelatin. It was important to make sure the Teflon sleeving was not too tight around the plastic mould, if no air can come through the bottom then the metal rods cannot be removed easily creating air-bubbles leading to attenuation artefacts. Three removable metal rods were placed in each mould.

Clear gelatin was allowed to set at room temperature around the metal rods, which were then carefully removed. Evans Blue (T-1824), an azo dye which is both optically absorbing and fluorescent, was used to provide optical contrast. Small amounts of Evans blue were added progressively to gelatin which was kept at 30deg using a heater-stirrer. The Evans blue doped gelatin was injected into the inclusions left by the metal rods using a 1ml syringe. A cuvette of each concentration of Evans blue gelatin was filled and allowed to set. The optical absorbance of each cuvette was measured using a spectrophotometer (REF). Phantom A had 3mm diameter inclusions and phantom B, 2mm inclusions, with increasing Evans Blue concentrations.

The phantoms were scanned under the same imaging conditions. The matching liquid used was 4.5% salt solution ( $RI \approx 1.341$ ) which gives a closer refractive index match than water. The average reconstructed pixel value of each finger was calculated from a single axial slice and averaged over a  $25 \times 25$  pixel area within the inclusion (see Figure 2.8b). As can be seen in Figure 2.8c, the reconstructed

pixel value of the optical CT system is linearly related to the optical absorbance as measured by spectrophotometer. The use of two phantoms verifies the linear relationship and the repeatability of measurements.

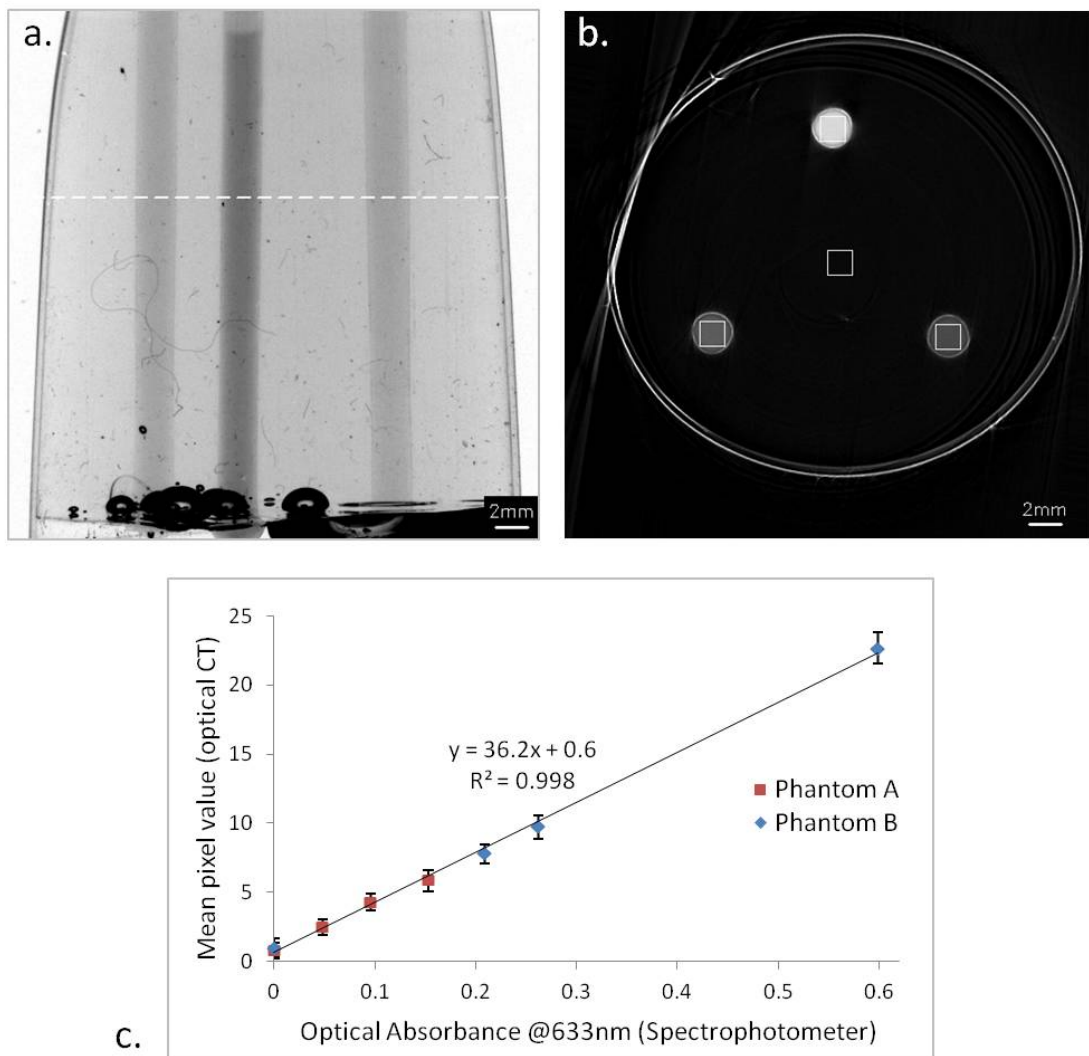


**Figure 2.8.** a. An optical CT projection image of a gelatin phantom containing 'finger' inclusions of different concentrations of Evans blue-dyed gel. b. A reconstructed slice through the phantom in the axial position marked by the dashed line in (a). Regions of Interest (ROIs) mark where the mean pixel value was calculated for each finger and the clear gelatin. The double ring artefact is due to refractive index mismatch between gel and the Teflon FEP container, and also between the Teflon and 4.5% saline solution matching liquid. c. Plot of absorbance of Evans Blue-doped gel measured with a Spectrophotometer against mean pixel value of different regions on reconstructed optical CT images. Two phantoms were measured with all variables constant between readings.

We expected that once the absorbance is too high the system response will drop off

non-linearly due to a lack of photons. This was demonstrated with a PRESAGE sample containing very large doses of radiation. Show graph of L3?

### 2.2.2 Spatial resolution

Understanding the spatial resolution response of the optical CT system is very important for acquiring high-quality, quantitative images. Previous publications noted a reduction of optical CT image contrast of small features as the feature size approaches the resolution. [Doran et al., 2013a] This effect is evident even when the feature size is several times the nominal spatial resolution and leads to non-linear response to optical absorbance. Therefore, the limits of spatial resolution of the system must be carefully characterised before we can be confident that measurements are quantitative.

There are many factors which can affect optical CT resolution (see theory section?). There is an added complexity when imaging extended objects as standard microscope lenses are designed to image a thin sample at the focal plane. For optical CT the spatial resolution either side of the focal plane is important as ideally the entire sample should be in focus at all times (see Figure 2.9). The distance over which the focus is ‘acceptable’ is known as the depth-of-field (DOF).

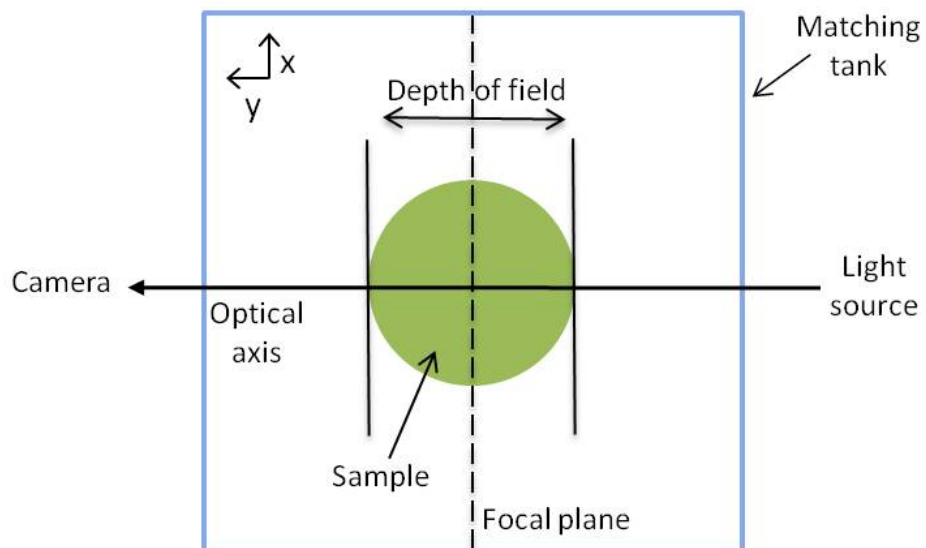


**Figure 2.9.** Schematic of the optical CT system geometry showing the ideal positions of the focal plane and depth-of-field.

Our optical system consists of components from a modular microscope system. This includes a zoom lens, giving variable magnification settings, and a variable

aperture which controls the DOF of the system. The aperture size can determine the overall acceptance angle of the optical system,  $\theta$ , which in turn affects the numerical aperture (NA), defined as  $N_A = n \sin \theta$ . A system with high NA results in high resolution,  $\Delta x$  (Equation 2.1). However, such a system has a small DOF due to the inverse relationship between DOF and NA (Equation 2.2).

$$\Delta x = \frac{0.61n\lambda}{N_A} \quad (2.1)$$

$$d_{DOF} = n_{bath} \left( \frac{n\lambda}{N_A^2} + \frac{ne}{MN_A} \right) = \frac{n_{bath}}{0.61n\lambda} \left( \Delta x^2 + \frac{ne}{M} \Delta x \right) \quad (2.2)$$

where  $n$ , the refractive index of the medium around the lens,  $n_{bath}$  the refractive index of the medium surrounding the sample,  $M$  the lateral magnification of the system,  $e$  the pixel size of the camera and  $\lambda$ , the wavelength of light.

To investigate the effect of changing the NA of our system we measured the modulation transfer function (MTF) for a range of positions along the optical axis. Five different NA values were evaluated, corresponding to the five reproducible aperture size settings on the lens system, labelled as A=1 to A=5, with A=1 being the smallest aperture and A=5 being the fully open aperture setting.

The modulation transfer function (MTF) characterises the resolution of a system by measuring how different spatial frequencies are transmitted. It is the Fourier transform of the Point Spread Function (PSF), giving a more comprehensive description of an optical system than quoting a single resolution value. There are various methods of measuring the MTF including simulating a point source or measuring the response to a sinusoidal pattern. These methods require test objects accurate to sub-pixel distances. It is much easier to manufacture an accurate sharp edge rather than a point source or slit. It has been shown that the MTF can be calculated analytically from the Edge Spread Function (ESF) as follows,

$$MTF(f) = \mathcal{F} [LSF(x)] = \mathcal{F} \left[ \frac{d}{dx} ESF(x) \right] \quad (2.3)$$

where  $f$  is spatial frequency,  $x$  is displacement and LSF is the Line Spread Function given by the profile of a slit source. [Boone et al., 1986]

Any noise in the data is amplified through the derivative and Fourier transform. Therefore, following the method of Boone *et al.*, the MTF was calculated directly from the fit parameters of a function fitted directly to measured ESF data. [Boone and Seibert, 1994] Analysis was carried out in IDL using curve fitting function ‘mpfit’. [Markwardt, 2009]

A knife edge was positioned at the focal plane and 50 projection images of matrix size  $2048 \times 2048$  were acquired and averaged to improve the signal-to-noise ratio (SNR). The knife edge was moved in steps of 0.1mm away from the focal plane in both directions along the optical axis. Images were acquired over a distance of 0.5mm in each direction giving a total distance of 1mm, the same as the FOV of each projection image. This was repeated for each aperture setting of the microscope lens.

Plotting the MTF at each position along the optical axis as an image, the DOF is visualised in a similar manner to [Chen et al., 2012a]. The maximum resolution for each NA was taken as the largest spatial frequency with continuous MTF values over 0.1 over some y-range, being the DOF for that resolution.

The MTF was calculated from ESF data, as seen in Figure 2.10, for a range of magnifications, pixel binning and LED voltages. The results in Figures 2.11 show that system response varies significantly with these variables as is expected. Magnifications of 0.8, 1 and 8 were tested to demonstrate the worst, standard and best conditions for imaging respectively.

The MTF was calculated from the ESF, measured across the centre of the knife-edge images, according to equation ? for each position along the optical axis and for each NA value. The MTF was represented by a grey level in a 2-D image in which the horizontal coordinate corresponds to spatial frequency, up to the desired  $100\text{mm}^{-1}$  (equivalent to a  $10\mu\text{m}$  line-pair), and the vertical coordinate corresponds to position along the optical axis. This allows visualisation of the DOF for each of the different NA values. The maximum resolution and corresponding DOF were measured for each NA setting. The maximum resolution was defined as the largest spatial frequency with an MTF above 10% at the focal plane. The DOF for this frequency was defined as the distance along the optical axis for which this spatial frequency had an MTF above 10%.

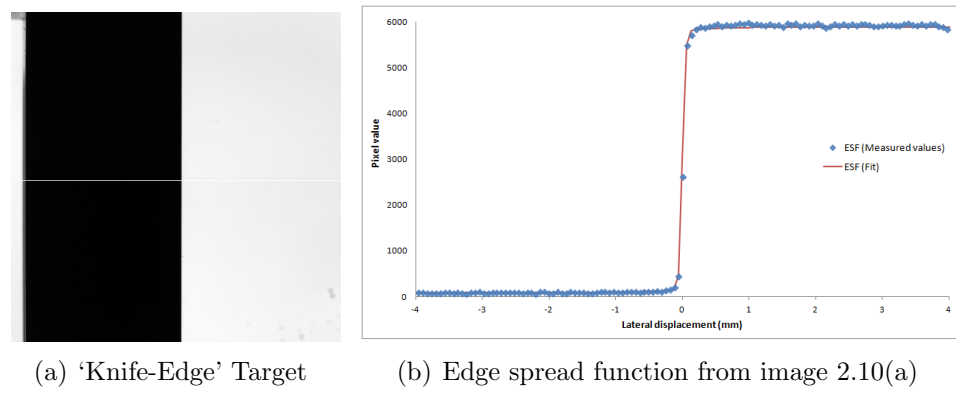


**Figure 2.10.** Image of a rectangular metal target with a straight edge which approximates a ‘Knife’ edge for the measurement of the Edge Spread Function (ESF, 2.10(b)). The pixel row across which the ESF is measured is marked on the image. This data was cropped to give 300 points centred on the edge to allow a curve to be fitted to the data accurately. Pixel size was measured allowing the pixel values to be plotted against displacement. The point of zero displacement was set at the edge for convenience in fitting a curve to the data. The MTF is calculated directly from the ESF via fit parameters.

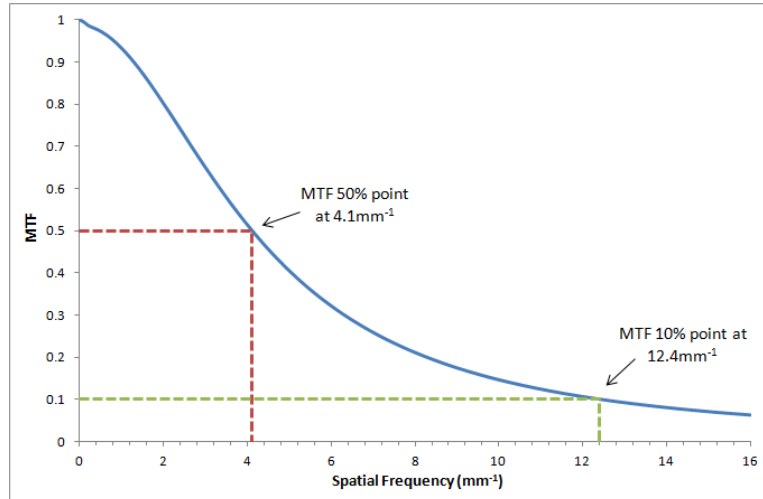


**Figure 2.11.** MTF vs spatial frequency for the case of  $M=1$ ,  $4 \times 4$  binning to  $512 \times 512$  pixels and LED voltage set to just below camera saturation levels, representing the imaging conditions for most phantom images in this report. The 50% cut-off point for the MTF, a value commonly quoted as giving the best focus is found to be  $4.1\text{mm}^{-1}$ . The 10% MTF value is  $12.4\text{mm}^{-1}$  and in general this value indicates the highest frequency that can be resolved by the system. This implies that features smaller than  $40\mu\text{m}$  will not be resolved at this magnification and binning.

The observed DOF and resolution results are shown in Table... and images of

MTF against optical axis position are shown in Figure REF. It is apparent that for low NA, there is a constant, low resolution across the entire FOV whereas at high NA there is a small region of high-resolution with other areas being defocused.

These results indicate that aperture settings must be chosen carefully for each imaging application. For most cases a constant resolution across the FOV is desirable, therefore A=1 is appropriate. For some cases, it may be desirable to have very high resolution in a small area around the centre of rotation in which case a higher aperture setting may be appropriate. However, positioning of the focal plane is very sensitive, illustrated through the use of a ‘point’ object test phantom containing  $5\mu\text{m}$  beads (Figure REF), it is apparent that the focal plane is not at the centre of the object. It is possible to attach this bead phantom to the bottom of other samples which gives us the ability to quantify how the resolution changes over the FOV.

Ideally the DOF of projection images should be larger than or equal to the sample size, as demonstrated in Figure 2.9. However, there is a trade-off between DOF and resolution,  $\Delta x$ , given by [Inoué and Spring, 1997b] as follows,

$$DOF = \frac{n_{bath}}{0.61n\lambda} (\Delta x^2 + \frac{ne}{M_{lat}}\Delta x) \quad (2.4)$$

where,  $n_{bath}$  is the refractive index of the medium surrounding the sample,  $n$  is the refractive index of the medium around the lens,  $\lambda$  is the wavelength of light,  $e$  is the pixel size of the camera and  $M_{lat}$  is the lateral magnification of the system. The DOF of the system can be adjusted by adjusting the overall acceptance angle of the system,  $\theta$ , which in turn controls the numerical aperture (NA) and this is inversely proportional to the resolution,

$$NA = n \sin \theta = \frac{0.61n\lambda}{\Delta x} \quad (2.5)$$

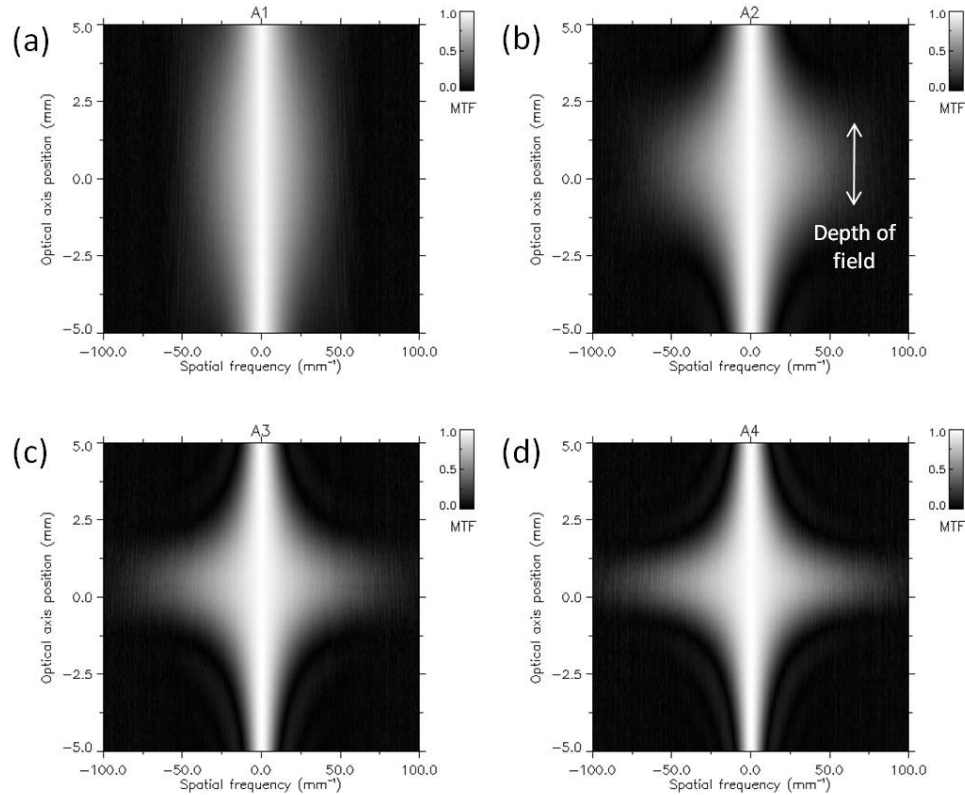


**Figure 2.12.** Measurements of the modulation transfer function (MTF) along the optical axis for different numerical aperture (NA) settings of the system, (a) A1 (b) A2 (c) A3 (d) A4. This allows visualisation of the depth-of-field (DOF).

NA setting	Resolution ( $\mu\text{m}$ )	Depth of field (mm)
A1	$21.5 \pm 0.5$	$9.3 \pm 0.4$
A2	$13.7 \pm 0.1$	$2.4 \pm 0.2$
A3	$12.0 \pm 0.2$	$1.6 \pm 0.2$
A4	$10.1 \pm 0.2$	$0.6 \pm 0.1$
A5	$9.7 \pm 0.2$	$0.4 \pm 0.1$

**Table 2.2.** Maximum resolution and corresponding depth-of-fields for different NA settings on the optical CT system. The uncertainties reflect noise in the modulation transfer function (MTF) measurements.

These measurements were all taken in ‘projection’ space and do not take into account the effect of the reconstruction process on resolution.

Bead phantom construction. A=5, m=8, sum 50 slices to get good visualisation

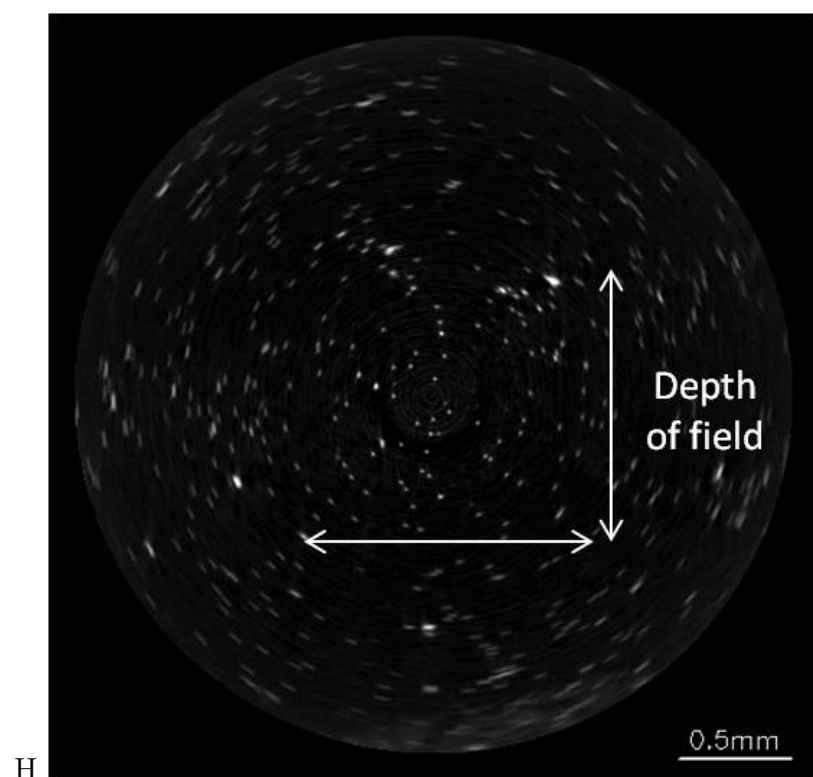


**Figure 2.13.** Bead imgs

# Bibliography

- [Abdul Rahman et al., 2011a] Abdul Rahman, A., Elke, B., Brochard, T., Adamovics, J., Clowes, S., Bradley, D., and Doran, S. J. (2011a). Sophisticated test objects for the quality assurance of optical computed tomography scanners. *Physics in medicine and biology*, 56(14):4177–4199.
- [Abdul Rahman et al., 2011b] Abdul Rahman, A. T., Bräuer-Krisch, E., Brochard, T., Adamovics, J., Clowes, S. K., Bradley, D., and Doran, S. J. (2011b). Sophisticated test objects for the quality assurance of optical computed tomography scanners. *Physics in Medicine and Biology*, 56(14):4177–4199.
- [Adamovics and Maryanski, 2003] Adamovics, J. and Maryanski, M. (2003). New 3d radiochromic solid polymer dosimeter from leuco dyes and a transparent polymeric matrix. In *Medical Physics*, volume 30, pages 1349–1349. AMER ASSOC PHYSICISTS MEDICINE AMER INST PHYSICS STE 1 NO 1, 2 HUNTINGTON QUADRANGLE, MELVILLE, NY 11747-4502 USA.
- [Akselrod et al., 2006] Akselrod, G., Akselrod, M., Benton, E., and Yasuda, N. (2006). A novel  $\text{al}_2\text{o}_3$  fluorescent nuclear track detector for heavy charged particles and neutrons. *Nuclear Instruments and Methods in Physics Research Section B: Beam Interactions with Materials and Atoms*, 247(2):295–306.
- [Anderson et al., 2003] Anderson, H. L., Yap, J. T., Miller, M. P., Robbins, A., Jones, T., and Price, P. M. (2003). Assessment of pharmacodynamic vascular response in a phase i trial of combretastatin a4 phosphate. *Journal of clinical oncology : official journal of the American Society of Clinical Oncology*, 21(15):2823–2830.
- [Annabell et al., 2012] Annabell, N., Yagi, N., Umetani, K., Wong, C., and Geso, M. (2012). Evaluating the peak-to-valley dose ratio of synchrotron microbeams using PRESAGE fluorescence. *Journal of synchrotron radiation*, 19(Pt 3):332–339.

- [Appleby et al., 1987] Appleby, A., Christman, E., and Leghrouz, A. (1987). Imaging of spatial radiation dose distribution in agarose gels using magnetic resonance. *Medical physics*, 14(3):382–384.
- [Asayesh et al., 2006] Asayesh, A., Sharpe, J., Watson, R. P., Hecksher-Sørensen, J., Hastie, N. D., Hill, R. E., and Ahlgren, U. (2006). Spleen versus pancreas: strict control of organ interrelationship revealed by analyses of bapx1/ mice. *Genes & Development*, 20(16):2208–2213.
- [Baldock et al., 2010] Baldock, C., De Deene, Y., Doran, S., Ibbott, G., Jirasek, A., Lepage, M., McAuley, K., Oldham, M., and Schreiner, L. (2010). Polymer gel dosimetry. *Physics in medicine and biology*, 55(5):R1.
- [Bassi et al., 2010] Bassi, A., Brida, D., D’Andrea, C., Valentini, G., Cubeddu, R., De Silvestri, S., and Cerullo, G. (2010). Time-gated optical projection tomography. *Optics letters*, 35(16):2732–2734.
- [Bayreder et al., 2008] Bayreder, C., Schon, R., Wieland, M., Georg, D., Moser, E., and Berg, A. (2008). The spatial resolution in dosimetry with normoxic polymer-gels investigated with the dose modulation transfer approach. *Medical physics*, 35(5):1756–1769.
- [Berg et al., 2004] Berg, A., Pernkopf, M., Waldhausl, C., Schmidt, W., and Moser, E. (2004). High resolution MR based polymer dosimetry versus film densitometry: a systematic study based on the modulation transfer function approach. *Physics in medicine and biology*, 49(17):4087–4108.
- [Blasberg, 2003] Blasberg, R. (2003). Molecular imaging and cancer. *Molecular cancer therapeutics*, 2(3):335–43.
- [Boone et al., 1986] Boone, J. M., Arnold, B. A., and Seibert, J. A. (1986). Characterization of the point spread function and modulation transfer function of scattered radiation using a digital imaging system. *Medical physics*, 13:254.
- [Boone and Seibert, 1994] Boone, J. M. and Seibert, J. A. (1994). An analytical edge spread function model for computer fitting and subsequent calculation of the LSF and MTF. *Medical Physics*, 21(10):1541–5.
- [Boot et al., 2008] Boot, M. J., Westerberg, C. H., Sanz-Ezquerro, J., Cotterell, J., Schweitzer, R., Torres, M., and Sharpe, J. (2008). In vitro whole-organ imaging: 4D quantification of growing mouse limb buds. *Nature Methods*, 5(7):609–612.

- [Bräuer-Krisch et al., 2003] Bräuer-Krisch, E., Bravin, A., Lerch, M., Rosenfeld, A., Stepanek, J., Di Michiel, M., and Laissue, J. (2003). Mosfet dosimetry for microbeam radiation therapy at the european synchrotron radiation facility. *Medical physics*, 30(4):583–589.
- [Bräuer-Krisch et al., 2013] Bräuer-Krisch, E., Nemoz, C., Brochard, T., Berruyer, G., Renier, M., Pouyatos, B., and Serduc, R. (2013). The preclinical set-up at the id17 biomedical beamline to achieve high local dose deposition using interlaced microbeams. In *Journal of Physics: Conference Series*, volume 425, page 022001. IOP Publishing.
- [Bräuer-Krisch et al., 2009] Bräuer-Krisch, E., Requardt, H., Brochard, T., Berruyer, G., Renier, M., Laissue, J., and Bravin, A. (2009). New technology enables high precision multislit collimators for microbeam radiation therapy. *Review of Scientific Instruments*, 80(7):074301.
- [Bräuer-Krisch et al., 2010] Bräuer-Krisch, E., Rosenfeld, A. B., Lerch, M. L., Petasecca, M., Akselrod, M., Sykora, J., Bartz, J., Ptaszkiewicz, M., Olko, P., and Berg, A. (2010). Potential high resolution dosimeters for MRT. *AIP Conference Proceedings*, 1266:89–97.
- [Brown et al., 1992] Brown, C. S., Burns, D. H., Spelman, F. A., and Nelson, A. C. (1992). Computed tomography from optical projections for three-dimensional reconstruction of thick objects. *Applied optics*, 31(29):6247–6254.
- [Chen et al., 2012a] Chen, L., James, M., Taylor, H. B., Bugeon, L., Lamb, J. R., Dallman, M. J., and French, P. M. (2012a). Incorporation of an experimentally determined MTF for spatial frequency filtering and deconvolution during optical projection tomography reconstruction. *Optics express*, 20(7):7323–7337.
- [Chen et al., 2012b] Chen, L., McGinty, J., Taylor, H. B., Bugeon, L., Lamb, J. R., Dallman, M. J., and French, P. M. W. (2012b). Incorporation of an experimentally determined MTF for spatial frequency filtering and deconvolution during optical projection tomography reconstruction. *Optics Express*, 20(7):7323–7337.
- [Chen et al., 2009] Chen, W.-S., Huang, R.-H., and Hsieh, L. (2009). Iris recognition using 3d co-occurrence matrix. In *Advances in Biometrics*, pages 1122–1131. Springer.
- [Choi et al., 2005] Choi, B., Tsu, L., Chen, E., Ishak, T. S., Iskandar, S. M., Chess, S., and Nelson, J. S. (2005). Determination of chemical agent optical

- clearing potential using in vitro human skin. *Lasers in Surgery and Medicine*, 36(2):72–75.
- [Clift et al., 2010] Clift, C., Thomas, A., Adamovics, J., Chang, Z., Das, I., and Oldham, M. (2010). Toward acquiring comprehensive radiosurgery field commissioning data using the presage®/optical-ct 3d dosimetry system. *Physics in medicine and biology*, 55(5):1279.
- [Colas and Sharpe, 2009] Colas, J. F. and Sharpe, J. (2009). Live optical projection tomography. *Organogenesis*, 5(4):211–216.
- [Crosbie et al., 2008] Crosbie, J., Svalbe, I., Midgley, S., Yagi, N., Rogers, P., and Lewis, R. (2008). A method of dosimetry for synchrotron microbeam radiation therapy using radiochromic films of different sensitivity. *Physics in medicine and biology*, 53(23):6861.
- [Crosbie et al., 2010] Crosbie, J. C., Anderson, R. L., Rothkamm, K., Restall, C. M., Cann, L., Ruwanpura, S., Meachem, S., Yagi, N., Svalbe, I., Lewis, R. A., et al. (2010). Tumor cell response to synchrotron microbeam radiation therapy differs markedly from cells in normal tissues. *International Journal of Radiation Oncology\* Biology\* Physics*, 77(3):886–894.
- [Cullis et al., 2006] Cullis, E. R., Kalber, T. L., Ashton, S. E., Cartwright, J. E., Griffiths, J. R., Ryan, A. J., and Robinson, S. P. (2006). Tumour overexpression of inducible nitric oxide synthase (iNOS) increases angiogenesis and may modulate the anti-tumour effects of the vascular disrupting agent ZD6126. *Microvascular research*, 71(2):76–84.
- [Darrell et al., 2008] Darrell, A., Meyer, H., Marias, K., Brady, M., and Ripoll, J. (2008). Weighted filtered backprojection for quantitative fluorescence optical projection tomography. *Physics in Medicine and Biology*, 53(14):3863–3881.
- [Doran et al., 2013a] Doran, S., Rahman, A. A., Bräuer-Krisch, E., Brochard, T., and Adamovics, J. (2013a). Ultra-high resolution optical ct dosimetry for the visualisation of synchrotron microbeam therapy doses. In *Journal of Physics: Conference Series*, volume 444, page 012074. IOP Publishing.
- [Doran, 2009a] Doran, S. J. (2009a). The history and principles of optical computed tomography for scanning 3-D radiation dosimeters: 2008 update. *Journal of Physics: Conference Series*, 164.
- [Doran, 2009b] Doran, S. J. (2009b). The history and principles of optical computed tomography for scanning 3-D radiation dosimeters: 2008 update. *Journal*

- of Physics: Conference Series*, 164:012020.
- [Doran et al., 2013b] Doran, S. J., Abdul Rahman, A., Brauer-Krisch, E., Brochard, T., Adamovics, J., Nisbet, A., and Bradley, D. (2013b). Establishing the suitability of quantitative optical CT microscopy of PRESAGE® radiochromic dosimeters for the verification of synchrotron microbeam therapy. *Physics in medicine and biology*, 58(18):6279–6297.
- [Doran et al., 2010a] Doran, S. J., Brochard, T., Adamovics, J., Krstajić, N., and Bräuer-Krisch, E. (2010a). An investigation of the potential of optical computed tomography for imaging of synchrotron-generated x-rays at high spatial resolution. *Physics in Medicine and Biology*, 55(5):1531–1547.
- [Doran et al., 2010b] Doran, S. J., Brochard, T., Adamovics, J., Krstajic, N., and Elke, B. (2010b). An investigation of the potential of optical computed tomography for imaging of synchrotron-generated x-rays at high spatial resolution. *Physics in medicine and biology*, 55(5):1531–1547.
- [Doran et al., 2001] Doran, S. J., Koerkamp, K. K., Bero, M. A., Jenneson, P., Morton, E. J., and Gilboy, W. B. (2001). A CCD-based optical CT scanner for high-resolution 3D imaging of radiation dose distributions: equipment specifications, optical simulations and preliminary results. *Physics in Medicine and Biology*, 46(12):3191–3213.
- [Doubrovin et al., 2001] Doubrovin, M., Ponomarev, V., Beresten, T., Balatoni, J., Bornmann, W., Finn, R., Humm, J., Larson, S., Sadelain, M., Blasberg, R., and et al. (2001). Imaging transcriptional regulation of p53-dependent genes with positron emission tomography in vivo. *Proceedings of the National Academy of Sciences of the United States of America*, 98(16):93005.
- [E et al., 2010] E, B., Serduc, R., Siegbahn, E., Le Duc, G., Prezado, Y., Bravin, A., Blattmann, H., and Laissue, J. (2010). Effects of pulsed, spatially fractionated, microscopic synchrotron x-ray beams on normal and tumoral brain tissue. *Mutation research*, 704(1-3):160–166.
- [Evelhoch et al., 2004] Evelhoch, J. L., M, L. P., He, Z., Zachary, D., Polin, L., Corbett, T. H., Langmuir, P., Wheeler, C., Stone, A., Leadbetter, J., Ryan, A. J., Blakey, D. C., and Waterton, J. C. (2004). Magnetic resonance imaging measurements of the response of murine and human tumors to the vascular-targeting agent ZD6126. *Clinical cancer research : an official journal of the American Association for Cancer Research*, 10(11):3650–3657.

- [Fauver et al., 2005a] Fauver, M., Seibel, E., Rahn, J., Meyer, M., Patten, F., Neumann, T., and Nelson, A. (2005a). Three-dimensional imaging of single isolated cell nuclei using optical projection tomography. *Optics express*, 13(11):4210–4223.
- [Fauver et al., 2005b] Fauver, M., Seibel, E. J., Rahn, J. R., Meyer, M. G., Patten, F. W., Neumann, T., and Nelson, A. C. (2005b). Three-dimensional imaging of single isolated cell nuclei using optical projection tomography. *Opt. Express*, 13(11):4210–4223.
- [Fei et al., 2012] Fei, P., Yu, Z., Wang, X., Lu, P. J., Fu, Y., He, Z., Xiong, J., and Huang, Y. (2012). High dynamic range optical projection tomography (HDR-OPT). *Optics Express*, 20(8):8824–8836.
- [Gore et al., 1996] Gore, J., Ranade, M., Maryański, M., and Schulz, R. (1996). Radiation dose distributions in three dimensions from tomographic optical density scanning of polymer gels: I. development of an optical scanner. *Physics in medicine and biology*, 41(12):2695–2704.
- [Gore et al., 1999] Gore, J. C., Ranade, M., and Maryanski, M. J. (1999). Radiation dose distributions in three dimensions from tomographic optical density scanning of polymer gels: I. Development of an optical scanner - Abstract - Physics in Medicine and Biology - IOPscience. *Physics in medicine* ....
- [Groom, 1987] Groom, A. (1987). The microcirculatory society eugene m. landis award lecture. microcirculation of the spleen: new concepts, new challenges. *Microvascular research*, 34(3):269–289.
- [Gross and Piwnica-Worms, 2005] Gross, S. and Piwnica-Worms, D. (2005). Spying on cancer: molecular imaging in vivo with genetically encoded reporters. *Cancer cell*, 7(1):5–15.
- [Guffroy et al., 2004] Guffroy, M., Dally, C., Vrignaud, P., Beys, E., and Bissery, M. (2004). Evaluation of tissue perfusion (tumor, spleen, heart) in mice after administration of AVE8062, a tumor vascular-targeting agent. *Proceedings of the American Association for Cancer Research*, 2004(1):1255.
- [Guo et al., 2006] Guo, P., Adamovics, J., and Oldham, M. (2006). A practical three-dimensional dosimetry system for radiation therapy. *Medical Physics*, 33(10):3962.
- [Hanahan and Weinberg, 2000] Hanahan, D. and Weinberg, R. A. (2000). The hallmarks of cancer. *Cell*, 100(1):57–70.

- [Haralick et al., 1973] Haralick, R. M., Shanmugam, K., and Dinstein, I. H. (1973). Textural features for image classification. *Systems, Man and Cybernetics, IEEE Transactions on*, 6:610–621.
- [Häusler, 1972] Häusler, G. (1972). A method to increase the depth of focus by two step image processing. *Optics Communications*, 6(1):38–42.
- [Hecht, 2002] Hecht, E. (2002). *Optics*. Addison-Wesley.
- [Hecksher-Sørensen et al., 2004] Hecksher-Sørensen, J., Watson, R. P., Lettice, L. A., Serup, P., Eley, L., De Angelis, C., Ahlgren, U., and Hill, R. E. (2004). The splanchnic mesodermal plate directs spleen and pancreatic laterality, and is regulated by *Bapx1/Nkx3.2*. *Development*, 131(19):4665–4675.
- [Heilemann et al., 2015] Heilemann, G., Georg, D., and Berg, A. (2015). Pushing the boundaries of spatial resolution in dosimetry using polymer gels and radiochromic films. In *Journal of Physics: Conference Series*, volume 573, page 012034. IOP Publishing.
- [Hoffman, 2005] Hoffman, R. (2005). The multiple uses of fluorescent proteins to visualize cancer in vivo. *Nature reviews. Cancer*, 5(10):796–806.
- [Hoffman, 2009] Hoffman, R. M. (2009). Imaging cancer dynamics in vivo at the tumor and cellular level with fluorescent proteins. *Clinical and Experimental Metastasis*, 26:345–355.
- [Hörnblad et al., 2011] Hörnblad, A., Cheddad, A., and Ahlgren, U. (2011). An improved protocol for optical projection tomography imaging reveals lobular heterogeneities in pancreatic islet and -cell mass distribution. *Islets*, 3(4):204–208.
- [Horsman and Murata, 2003] Horsman, M. R. and Murata, R. (2003). Vascular targeting effects of ZD6126 in a C3H mouse mammary carcinoma and the enhancement of radiation response. *International journal of radiation oncology, biology, physics*, 57(4):1047–1055.
- [Hsieh, 2003] Hsieh, J. (2003). *Computed Tomography: Principles, Design, Artifacts, and Recent Advances*. SPIE Press monograph. SPIE Press.
- [Huang et al., 1993] Huang, D., Swanson, E. A., Lin, C. P., Schuman, J. S., Stinson, W. G., Chang, W., Hee, M. R., Flotte, T., Gregory, K., Puliafito, C. A., et al. (1993). *Optical coherence tomography*. PhD thesis, Massachusetts Institute of Technology, Whitaker College of Health Sciences and Technology.

- [Hudson and Larkin, 1994] Hudson, H. and Larkin, R. (1994). Accelerated image reconstruction using ordered subsets of projection data. *Medical Imaging, IEEE Transactions on*, 13(4):601–609.
- [Inoué and Spring, 1997a] Inoué, S. and Spring, K. R. (1997a). *Video Microscopy: The Fundamentals*. The Language of Science. Plenum Press.
- [Inoué and Spring, 1997b] Inoué, S. and Spring, K. R. (1997b). Video microscopy: The fundamentals (the language of science).
- [Islam et al., 2003] Islam, K. T. S., Dempsey, J. F., Ranade, M. K., Maryanski, M. J., and Low, D. A. (2003). Initial evaluation of commercial optical CT-based 3D gel dosimeter. *Medical Physics*, 30(8):2159.
- [Kawata et al., 1990] Kawata, S., Nakamura, O., Noda, T., Ooki, H., Ogino, K., Kuroiwa, Y., and Minami, S. (1990). Laser computed-tomography microscope. *Applied optics*, 29(26):3805–3809.
- [Kelly et al., 1998] Kelly, R. G., Jordan, K. J., and Battista, J. J. (1998). Optical CT reconstruction of 3D dose distributions using the ferrous–benzoic–xylene (FBX) gel dosimeter. *Medical Physics*, 25(9):1741–50.
- [Kim et al., 2008] Kim, E., Bowsher, J., Thomas, A. S., Sakhalkar, H., Dewhirst, M., and Oldham, M. (2008). Improving the quantitative accuracy of optical-emission computed tomography by incorporating an attenuation correction: application to HIF1 imaging. *Physics in Medicine and Biology*, 53(19):5371–5383.
- [Krstajić and Doran, 2006] Krstajić, N. and Doran, S. J. (2006). Focusing optics of a parallel beam CCD optical tomography apparatus for 3D radiation gel dosimetry. *Physics in Medicine and Biology*, 51(8):2055–2075.
- [Krstajić and Doran, 2007] Krstajić, N. and Doran, S. J. (2007). Characterization of a parallel-beam CCD optical-CT apparatus for 3D radiation dosimetry. *Physics in Medicine and Biology*, 52(13):3693–3713.
- [Krstajic and Doran, 2007] Krstajic, N. and Doran, S. J. (2007). Characterization of a parallel-beam CCD optical-CT apparatus for 3D radiation dosimetry. *Physics in medicine and biology*, 52(13):3693–3713.
- [Laissie et al., 2001] Laissie, J. A., Blattmann, H., Di Michiel, M., Slatkin, D. N., Lyubimova, N., Guzman, R., Zimmermann, W., Birrer, S., Bley, T., Kircher, P., et al. (2001). Weanling piglet cerebellum: a surrogate for toler-

- ance to mrt (microbeam radiation therapy) in pediatric neuro-oncology. In *International Symposium on Optical Science and Technology*, pages 65–73. International Society for Optics and Photonics.
- [Lerch et al., 2011] Lerch, M., Petasecca, M., Cullen, A., Hamad, A., Requardt, H., Bräuer-Krisch, E., Bravin, A., Perevertaylo, V., and Rosenfeld, A. B. (2011). Dosimetry of intensive synchrotron microbeams. *Radiation Measurements*, 46(12):1560–1565.
- [Lorbeer et al., 2011] Lorbeer, R. A., Heidrich, M., Lorbeer, C., Ramírez Ojeda, D. F., Bicker, G., Meyer, H., and Heisterkamp, A. (2011). Highly efficient 3D fluorescence microscopy with a scanning laser optical tomograph. *Optics Express*, 19(6):5419–5430.
- [Mao et al., 2008] Mao, Z., Zhu, D., Hu, Y., Wen, X., and Han, Z. (2008). Influence of alcohols on the optical clearing effect of skin in vitro. *Journal of Biomedical Optics*, 13(2):021104–021104.
- [Markwardt, 2009] Markwardt, C. B. (2009). Non-linear least squares fitting in idl with mpfit. *arXiv preprint arXiv:0902.2850*.
- [Martínez-Rovira et al., 2012] Martínez-Rovira, I., Sempau, J., and Prezado, Y. (2012). Development and commissioning of a monte carlo photon beam model for the forthcoming clinical trials in microbeam radiation therapy. *Medical physics*, 39(1):119–131.
- [Maryanski et al., 1993] Maryanski, M. J., Gore, J. C., Kennan, R. P., and Schulz, R. J. (1993). Nmr relaxation enhancement in gels polymerized and cross-linked by ionizing radiation: a new approach to 3d dosimetry by mri. *Magnetic resonance imaging*, 11(2):253–258.
- [Maryanski et al., 1999] Maryanski, M. J., Zastavker, Y. Z., and Gore, J. C. (1999). Radiation dose distributions in three dimensions from tomographic optical density scanning of polymer gels: II. optical properties of the bang polymer gel. *Physics in medicine and biology*, 41(12):2705.
- [McGinty et al., 2008] McGinty, J., Tahir, K. B., Laine, R., Talbot, C. B., Dunsby, C., Neil, M. A. A., Quintana, L., Swoger, J., Sharpe, J., and French, P. M. W. (2008). Fluorescence lifetime optical projection tomography. *Journal of Biophotonics*, 1(5):390–394.
- [McGinty et al., 2011] McGinty, J., Taylor, H. B., Chen, L., Bugeon, L., Lamb, J. R., Dallman, M. J., and French, P. M. W. (2011). In vivo fluorescence lifetime

- optical projection tomography. *Biomedical optics express*, 2(5):1340–1350.
- [McGrath et al., 2010] McGrath, J., Drummond, G., McLachlan, E., Kilkenny, C., and Wainwright, C. (2010). Guidelines for reporting experiments involving animals: the arrive guidelines. *British journal of pharmacology*, 160(7):1573–1576.
- [Natterer, 2001] Natterer, F. (2001). *The Mathematics of Computerized Tomography*. Classics in Applied Mathematics. Society for Industrial and Applied Mathematics.
- [Oldham, 2004] Oldham, M. (2004). Optical-CT scanning of polymer gels. *Journal of Physics: Conference Series*, 3:122–135.
- [Oldham et al., 2008a] Oldham, M., Sakhalkar, H., Oliver, T., Allan Johnson, G., and Dewhirst, M. (2008a). Optical clearing of unsectioned specimens for three-dimensional imaging via optical transmission and emission tomography. *Journal of Biomedical Optics*, 13(2):021113.
- [Oldham et al., 2008b] Oldham, M., Sakhalkar, H., Oliver, T., Allan Johnson, G., and Dewhirst, M. (2008b). Optical clearing of unsectioned specimens for three-dimensional imaging via optical transmission and emission tomography. *Journal of biomedical optics*, 13(2):021113.
- [Oldham et al., 2006] Oldham, M., Sakhalkar, H., Oliver, T., Wang, Y. M., Kirkpatrick, J., Cao, Y., Badea, C., Johnson, G. A., and Dewhirst, M. (2006). Three-dimensional imaging of xenograft tumors using optical computed and emission tomography. *Medical Physics*, 33(9):3193.
- [Oldham et al., 2007a] Oldham, M., Sakhalkar, H., Wang, Y. M., Guo, P., Oliver, T., Bentley, R., Vujaskovic, Z., and Dewhirst, M. (2007a). Three-dimensional imaging of whole rodent organs using optical computed and emission tomography. *Journal of Biomedical Optics*, 12(1):014009.
- [Oldham et al., 2007b] Oldham, M., Sakhalkar, H., Wang, Y. M., Guo, P., Oliver, T., Bentley, R., Vujaskovic, Z., and Dewhirst, M. (2007b). Three-dimensional imaging of whole rodent organs using optical computed and emission tomography. *Journal of biomedical optics*, 12(1):014009.
- [Oldham et al., 2003] Oldham, M., Siewersdson, J. H., Kumar, S., Wong, J., and Jaffray, D. A. (2003). Optical-CT gel-dosimetry I: basic investigations. *Medical Physics*, 30(4):623.

- [Oldham et al., 2001] Oldham, M., Siewerdsen, J. H., Shetty, A., and Jaffray, D. A. (2001). High resolution gel-dosimetry by optical-CT and MR scanning. *Medical Physics*, 28(7):1436.
- [Olding and Schreiner, 2011] Olding, T. and Schreiner, L. J. (2011). Cone-beam optical computed tomography for gel dosimetry II: imaging protocols. *Physics in Medicine and Biology*, 56(5):1259–1279.
- [Padhani and Miles, 2010] Padhani, A. R. and Miles, K. A. (2010). Multiparametric Imaging of Tumor Response to Therapy. *Radiology*, 256(2):348–364.
- [Pouyatos et al., 2013] Pouyatos, B., Serduc, R., Chipaux, M., Chabrol, T., Bräuer-Krisch, E., Nemoz, C., Mathieu, H., David, O., Renaud, L., Prezado, Y., et al. (2013). Synchrotron x-ray interlaced microbeams suppress paroxysmal oscillations in neuronal networks initiating generalized epilepsy. *Neurobiology of disease*, 51:152–160.
- [Ptaszkiewicz et al., 2008] Ptaszkiewicz, M., Braurer-Kirsch, E., Kłosowski, M., Czopyk, L., and Olko, P. (2008). Tld dosimetry for microbeam radiation therapy at the european synchrotron radiation facility. *Radiation Measurements*, 43(2):990–993.
- [Ragan et al., 1988] Ragan, D., Schmidt, E., IC, M., and Groom, A. (1988). Spontaneous cyclic contractions of the capillary wall in vivo, impeding red cell flow: a quantitative analysis. evidence for endothelial contractility. *Microvascular research*, 36(1):13–30.
- [Ray and Semerjian, 1983] Ray, S. R. and Semerjian, H. G. (1983). Laser tomography for simultaneous concentration and temperature measurement in reacting flows. In *American Institute of Aeronautics and Astronautics, Thermophysics Conference, 18 th, Montreal, Canada*.
- [Requardt et al., 2005] Requardt, H., Corde, S., Siegbahn, E., LeDuc, G., Brochard, T., Blattmann, H., Laissue, J., Bravin, A., et al. (2005). New irradiation geometry for microbeam radiation therapy. *Physics in medicine and biology*, 50(13):3103.
- [Rosset et al., 2004] Rosset, A., Spadola, L., and Ratib, O. (2004). OsiriX: an open-source software for navigating in multidimensional DICOM images. *Journal of Digital Imaging*, 17(3):205–216.
- [Russ, 2002] Russ, J. C. (2002). *The Image Processing Handbook*. Image Processing Handbook. Crc Press.

- [Sakhalkar et al., 2009] Sakhalkar, H. S., Adamovics, J., Ibbott, G., and Oldham, M. (2009). A comprehensive evaluation of the PRESAGE/optical-CT 3D dosimetry system. *Medical Physics*, 36(1):71.
- [Sakhalkar et al., 2007] Sakhalkar, H. S., Dewhirst, M., Oliver, T., Cao, Y., and Oldham, M. (2007). Functional imaging in bulk tissue specimens using optical emission tomography: fluorescence preservation during optical clearing. *Physics in Medicine and Biology*, 52(8):2035–2054.
- [Sakhalkar and Oldham, 2008] Sakhalkar, H. S. and Oldham, M. (2008). Fast, high-resolution 3D dosimetry utilizing a novel optical-CT scanner incorporating tertiary telecentric collimation. *Medical Physics*, 35(1):101.
- [Schreiner, 2004] Schreiner, L. (2004). Review of fricke gel dosimeters. In *Journal of Physics: Conference Series*, volume 3, page 9. IOP Publishing.
- [Serduc et al., 2009] Serduc, R., Bräuer-Krisch, E., Bouchet, A., Renaud, L., Brochard, T., Bravin, A., Laissue, J. A., and Le Duc, G. (2009). First trial of spatial and temporal fractionations of the delivered dose using synchrotron microbeam radiation therapy. *Synchrotron Radiation*, 16(4):587–590.
- [Serduc et al., 2010] Serduc, R., Elke, B., Siegbahn, E. A., Bouchet, A., Pouyatos, B., Carron, R., Pannetier, N., Renaud, L., Berruyer, G., Nemoz, C., Brochard, T., Rémy, C., Barbier, E. L., Bravin, A., Le Duc, G., Depaulis, A., Estève, F., and Laissue, J. A. (2010). High-precision radiosurgical dose delivery by interlaced microbeam arrays of high-flux low-energy synchrotron x-rays. *PloS one*, 5(2):e9028.
- [Sharpe, 2002] Sharpe, J. (2002). Optical Projection Tomography as a Tool for 3D Microscopy and Gene Expression Studies. *Science*, 296(5567):541–545.
- [Sharpe, 2003a] Sharpe, J. (2003a). Optical projection tomography as a new tool for studying embryo anatomy. *Journal of Anatomy*, 202(2):175–181.
- [Sharpe, 2003b] Sharpe, J. (2003b). Optical projection tomography as a new tool for studying embryo anatomy. *Journal of anatomy*, 202(2):175–181.
- [Sharpe et al., 2002] Sharpe, J., Ahlgren, U., Perry, P., Hill, B., Ross, A., Jacob, H., Baldock, R., and Davidson, D. (2002). Optical projection tomography as a tool for 3D microscopy and gene expression studies. *Science (New York, N.Y.)*, 296(5567):541–545.
- [Shcherbo et al., 2007] Shcherbo, D., Merzlyak, E., Chepurnykh, T., Fradkov,

- A., Ermakova, G., Solovieva, E., Lukyanov, K., Bogdanova, E., Zaraisky, A., Lukyanov, S., and et al. (2007). Bright far-red fluorescent protein for whole-body imaging. *Nature methods*, 4(9):741–6.
- [Siegbahn et al., 2009] Siegbahn, E., E. B., Bravin, A., Nettelbeck, H., Lerch, M., and Rosenfeld, A. (2009). MOSFET dosimetry with high spatial resolution in intense synchrotron-generated x-ray microbeams. *Medical physics*, 36(4):1128–1137.
- [Skyt et al., 2011] Skyt, P. S., Balling, P., Petersen, J. B. B., Yates, E. S., and Muren, L. P. (2011). Temperature dependence of the dose response for a solid-state radiochromic dosimeter during irradiation and storage. *Medical physics*, 38(5):2806–2811.
- [Skyt et al., 2012] Skyt, P. S., Wahlstedt, I., Muren, L. P., Petersen, J. B. B., and Balling, P. (2012). Temperature and temporal dependence of the optical response for a radiochromic dosimeter. *Medical physics*, 39(12):7232–7236.
- [Soufan et al., 2003] Soufan, A. T., Ruijter, J. M., van den Hoff, M. J. B., de Boer, P. A. J., Hagoort, J., and Moorman, A. F. M. (2003). Three-dimensional reconstruction of gene expression patterns during cardiac development. *Physiological genomics*, 13(3):187–195.
- [Tarte et al., 1996] Tarte, B. J., Jardine, P. A., and van Doorn, T. (1996). Laser-scanned agarose gel sections for radiation field mapping. *International Journal of Radiation Oncology\* Biology\* Physics*, 36(1):175–179.
- [Tarte et al., 1997] Tarte, B. J., Jardine, P. A., van Doorn, T., Nitschke, K. N., and Poulsen, M. G. (1997). Development of a CCD array imaging system for measurement of dose distributions in doped agarose gels. *Medical Physics*, 24:1521.
- [Thomas et al., 2010] Thomas, A., Bowsher, J., Roper, J., Oliver, T., Dewhirst, M., and Oldham, M. (2010). A comprehensive method for optical-emission computed tomography. *Physics in Medicine and Biology*, 55(14):3947–3957.
- [Thomas et al., 2011a] Thomas, A., Newton, J., and Oldham, M. (2011a). A method to correct for stray light in telecentric optical-CT imaging of radiochromic dosimeters. *Physics in Medicine and Biology*, 56(14):4433–4451.
- [Thomas et al., 2011b] Thomas, A., Pierquet, M., Jordan, K., and Oldham, M. (2011b). A method to correct for spectral artifacts in optical-CT dosimetry. *Physics in medicine and biology*, 56(11):3403–3416.

- [Tuchin and Engineers, 2007] Tuchin, V. V. and Engineers, S. O. P.-O. I. (2007). *Tissue Optics: Light Scattering Methods and Instruments for Medical Diagnosis*. Press Monographs. SPIE/International Society for Optical Engineering.
- [Tuchin et al., 2002] Tuchin, V. V., Xu, X., and Wang, R. K. (2002). Dynamic Optical Coherence Tomography in Studies of Optical Clearing, Sedimentation, and Aggregation of Immersed Blood. *Applied optics*, 41(1):258–271.
- [Vargas et al., 1999] Vargas, G., Chan, E. K., Barton, J. K., Rylander, H. G., and Welch, A. J. (1999). Use of an Agent to Reduce Scattering. *Lasers in Surgery and Medicine*, 24(2):133–41.
- [Varia et al., 1998] Varia, M., Calkins-Adams, D., Rinker, L., Kennedy, A., Novotny, D., Fowler, W., and Raleigh, J. (1998). Pimonidazole: a novel hypoxia marker for complementary study of tumor hypoxia and cell proliferation in cervical carcinoma. *Gynecologic oncology*, 71(2):270–277.
- [Varosi and Landsman, 1993] Varosi, F. and Landsman, W. (1993). An idl based image deconvolution software package. In *Astronomical Data Analysis Software and Systems II*, volume 52, page 515.
- [Vinegoni et al., 2008] Vinegoni, C., Pitsouli, C., Razansky, D., Perrimon, N., and Ntziachristos, V. (2008). In vivo imaging of *Drosophila melanogaster* pupae with mesoscopic fluorescence tomography. *Nature Methods*, 5(1):45–47.
- [Walls et al., 2005] Walls, J. R., Sled, J. G., Sharpe, J., and Henkelman, R. M. (2005). Correction of artefacts in optical projection tomography. *Physics in Medicine and Biology*, 50(19):4645–4665.
- [Walls et al., 2007] Walls, J. R., Sled, J. G., Sharpe, J., and Henkelman, R. M. (2007). Resolution improvement in emission optical projection tomography. *Physics in Medicine and Biology*, 52(10):2775–2790.
- [Wang and Wang, 2006] Wang, Y. and Wang, R. (2006). Imaging using parallel integrals in optical projection tomography. *Physics in Medicine and Biology*, 51(23):6023–6032.
- [Wang and Wang, 2007] Wang, Y. and Wang, R. K. (2007). Optimization of image-forming optics for transmission optical projection tomography. *Applied optics*, 46(27):6815–6820.
- [Webb, 1996] Webb, R. H. (1996). Confocal optical microscopy. *Reports on Progress in Physics*, 59:427–471.

- [Wen et al., 2009] Wen, X., Tuchin, V. V., Luo, Q., and Zhu, D. (2009). Controlling the scattering of Intralipid by using optical clearing agents. *Physics in Medicine and Biology*, 54(22):6917–6930.
- [Winfree et al., 1996a] Winfree, A. T., Caudle, S., Chen, G., McGuire, P., and Szilagyi, Z. (1996a). Quantitative optical tomography of chemical waves and their organizing centers. *Chaos: An Interdisciplinary Journal of Nonlinear Science*, 6(4):617–626.
- [Winfree et al., 1996b] Winfree, A. T., Caudle, S., Chen, G., P., M., and Szilagyi, Z. (1996b). Quantitative optical tomography of chemical waves and their organizing centers. *Chaos (Woodbury, N.Y.)*, 6(4):617–626.
- [Wolodzko et al., 1999] Wolodzko, J. G., Marsden, C., and Appleby, A. (1999). CCD imaging for optical tomography of gel radiation dosimeters. *Medical Physics*, 26:2508.
- [Workman et al., 2010] Workman, P., Aboagye, E., Balkwill, F., Balmain, A., Bruder, G., Chaplin, D., Double, J., Everitt, J., Farningham, D., Glennie, M., et al. (2010). Guidelines for the welfare and use of animals in cancer research. *British journal of cancer*, 102(11):1555–1577.
- [Xia et al., 1995] Xia, W., Lewitt, R., and Edholm, P. (1995). Fourier correction for spatially variant collimator blurring in spect. *Medical Imaging, IEEE Transactions on*, 14(1):100–115.
- [Xu et al., 2003] Xu, Y., Wuu, C., and Maryanski, M. J. (2003). Determining optimal gel sensitivity in optical CT scanning of gel dosimeters. *Medical Physics*, 30(8):2257.
- [Xu et al., 2004] Xu, Y., Wuu, C. S., and Maryanski, M. J. (2004). Performance of a commercial optical CT scanner and polymer gel dosimeters for 3-D dose verification. *Medical Physics*, 31(11):3024.
- [Yeh et al., 2003] Yeh, A. T., Choi, B., Nelson, J. S., and Tromberg, B. J. (2003). Reversible Dissociation of Collagen in Tissues. *The Journal of Investigative Dermatology*, 121(6):1332–5.
- [Zhu et al., 2013] Zhu, D., Larin, K. V., Luo, Q., and Tuchin, V. V. (2013). Recent progress in tissue optical clearing. *Laser & photonics reviews*, 7(5):732–757.